Nano-foaming of Polyamide Desalination Membranes to Tune Permeability and Selectivity

Xiao-Hua Ma[†, ‡], Zhi-Kan Yao[‡], Zhe Yang[‡], Hao Guo[‡], Zhen-Liang Xu[†], Chuyang Y. Tang*[,‡], Menachem Elimelech[§]

[†]Shanghai Key Laboratory of Multiphase Materials Chemical Engineering, East China University of Science and Technology, 130 Meilong Road, Shanghai, China

[‡]Department of Civil Engineering, The University of Hong Kong, Pokfulam HW619B, Hong Kong, China

[§]Department of Chemical and Environmental Engineering, Yale University, New Haven, CT 06520-8286

Email: *tangc@hku.hk; phone: +852 28591976; fax: +852 25595337.

ABSTRACT: Recent studies have documented the existence of discrete voids in the thin polyamide selective layer of composite reverse osmosis membranes. Here we show compelling evidence that these nanovoids are formed by nano-sized gas bubbles generated during the interfacial polymerization process. Different strategies were used to enhance or eliminate these nanobubbles in the thin polyamide film layer to tune its morphology and separation properties. Nanobubbles can endow the membrane with a foamed structure within the polyamide rejection layer of approximately 100 nm in thickness. Simple nano-foaming methods, such as bicarbonate addition and ultrasound application, can result in remarkable improvement in both membrane water permeability and salt rejection, thus overcoming the long-standing permeability-selectivity tradeoff of desalination membranes.

INTRODUCTION

Reverse osmosis technology plays a crucial role in providing alternative sources of water through desalination and water reclamation[1-3]. State-of-the-art reverse osmosis membranes are based on polyamide chemistry[4-6]. A typical polyamide membrane is fabricated by the interfacial polymerization of an amine monomer, *m*-phenylenediamine (MPD), and an acyl chloride monomer, trimesoyl chloride (TMC), to form a thin salt-rejecting film (typically 20-400 nm in thickness) on a porous substrate (**Figure 1A,B**)[7]. This thin polyamide film, which selectively removes ions and small molecules while enabling the permeation of water, largely determines the separation properties of the membrane. A recent study[8] demonstrated ultrafast solvent transport in a sub-10 nm polyamide nanofilm, with methanol flux showing two orders of magnitude improvement compared with commercially available organic solvent nanofiltration membranes.

The permeability and selectivity of a reverse osmosis membrane is strongly dependent on the morphology and structure of its thin polyamide film[9, 10]. Typically, the polyamide film has a surface roughness on the order of 100 nm due to the presence of "ridge-and-valley" structures[11, 12]. It is commonly believed that a rougher polyamide surface leads to greater water permeability due to increased membrane surface area[13, 14]. Careful characterization of the polyamide film revealed that the "ridge-and-valley" rough structures contain a large number of discrete nanovoids ranging in size from a few nanometers to approximately 100 nm (see **Figure 1C**)[7, 15-17]. These nanovoids can occupy as much as 30% of the volume within the polyamide rejection layer[17] and thus can contribute to the observed strong correlation between membrane permeability and surface roughness[18]. Recent molecular dynamic simulations also revealed the active role of these nanometer-scale pores in water filtration[7, 19].

Despite the critical importance of the nanovoids on membrane separation properties, their exact formation

mechanism is still largely unknown. A prevailing hypothesis is that these voids are formed by the encapsulation of water droplets inside the polyamide layer during interfacial polymerization[20, 21]. Nevertheless, this hypothesis cannot explain why the "ridge-and-valley" structures would be absent when low concentrations of amine and acyl chloride monomers are used[8].

We hypothesize that the nanovoids are formed due to the release of nano-sized gas bubbles during the interfacial polymerization process. **Figure 1A** shows the exothermic reaction of MPD and TMC to form a crosslinked polyamide rejection layer. The heat generated from the reaction reduces the solubility of dissolved gases such as CO_2, N_2, and O_2. At the same time, this reaction also produces a strong acid (HCl) as a byproduct, which can further facilitate the degassing of CO_2[22]. **Figure 1D** shows the inflation of a balloon by the gas released by mixing bulk solutions of MPD and TMC. In the context of interfacial polymerization, the released fine gas bubbles would be encapsulated as the crosslinked polyamide rapidly "freezes". We further show different strategies to enhance or eliminate the formation of nanobubbles for tuning the morphology and separation performance of the polyamide rejection layer. Our study provides in-depth understanding of the fundamental mechanisms involved in the formation of polyamide membranes and offers new dimensions for tailoring their structure and separation performance.

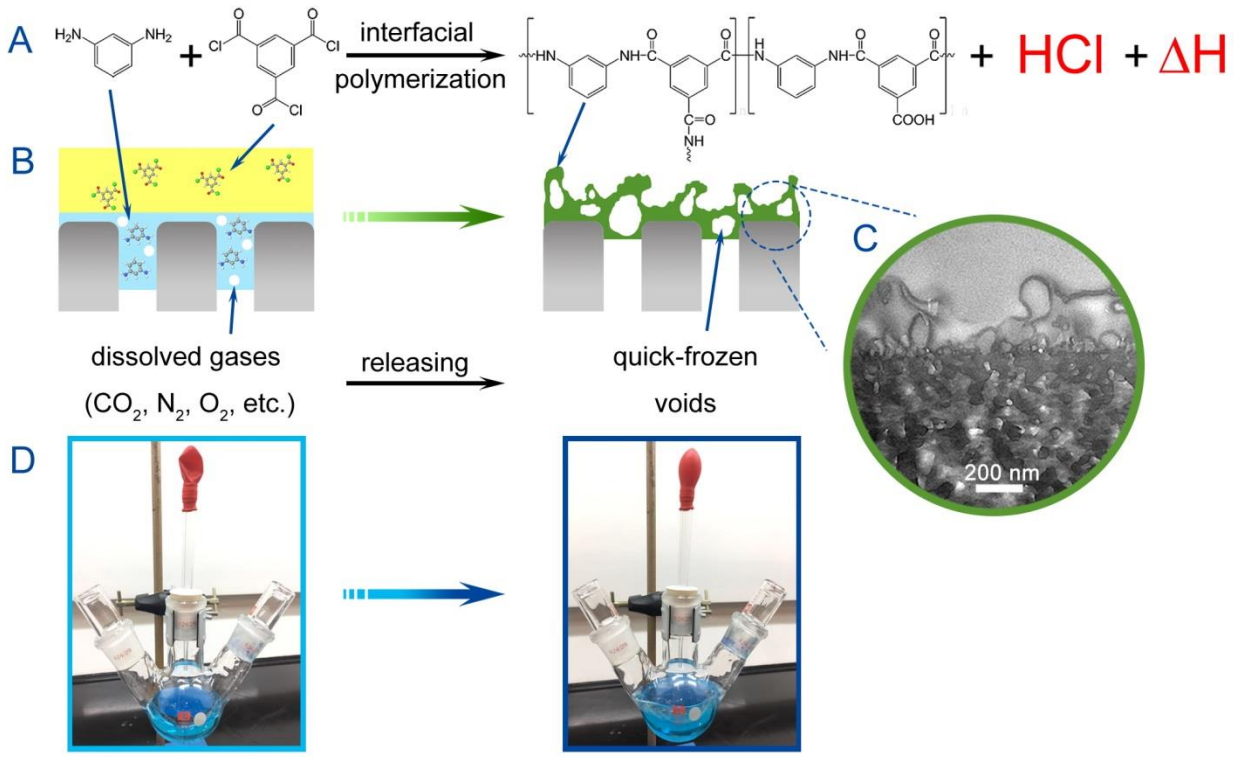

Figure 1. Interfacial polymerization process for the formation of a polyamide thin film. (A) Interfacial polymerization of *m*-phenylenediamine (MPD) and trimesoyl chloride (TMC) to form polyamide. HCl and heat are generated as by-products. (B) Nano-sized bubbles formed by the released dissolved gases from the monomer solution are quick-frozen in the polyamide thin film. (C) Transmission electron micrograph (TEM) cross-sectional image of a commercial reverse osmosis membrane (BW30) with discrete voids and "ridge-and-valley" morphology. (D) Inflation of a balloon by the gas released from the mixing of bulk solutions of MPD (dyed by methyl blue) and TMC.

MATERIALS AND METHODS

Characterization. Transmission electron microscopy (TEM) was carried out using Philips CM100 TEM. A membrane coupon was firstly embedded in LR white resin. Samples of TEM cross-section were obtained by sectioning the resin block with an ultramicrotome equipped with a diamond knife. The resulting cross-sections were mounted onto carbon-coated TEM grids for imaging. Polyamide thin film composite membrane with enhanced or eliminated nanobubbles were analyzed by scanning electron microscopy (SEM) using Hitachi S4800 FEG SEM. Samples were sputtered with a uniform layer of gold of approximately 6 nm before SEM characterization. Atomic force microscopy (AFM, Veeco NanoScope AFM) was used to measure the surface

roughness of the polyamide membranes. The obtained AFM images were analyzed using Gwyddion software. Hong Kong Baptist University provided the X-ray photoelectron spectroscopy (XPS) characterization using an SKL-12 spectrometer (Leybold, Sengyang, China) equipped with a VG CLAM 4 MCD electron energy analyzer. Data processing was performed using CasaXps.

Interfacial polymerization on a support substrate is a well-known technique to fabricate reverse osmosis membranes. In the current work, we prepared polyamide membranes at "high concentration" and "low conctration" for comparison.

Polyamide membrane at "high concentration". MPD flakes were added in Milli-Q water to prepare an aqueous solution with a concentration of 2.0 wt.%. TMC was added in hexane to prepare an organic solution with a concentration of 0.2 wt.%. These concentrations are typical for the synthesis of commercial reverse osmosis desalination membranes by interfacial polymerization. The MPD aqueous solution was poured on the top surface of polysulfone substrate. After soaking for 2 min, the excess aqueous solution was carefully removed from the polysulfone top surface using a rubber roller. The TMC hexane solution was then gently poured onto the aqeuous solution-soaked polysulfone substrate and the interfacial polymerization reaction was continued for 2 min. A thin polyamdie film was formed on the polysulfone substrate. After the reaction, the thin polyamide layer was cleaned with a sufficient amount of hexane and the membrane was put in warm deionized water at 50 °C for 10 min. Finally, the polyamide thin film composite membrane was stored in deionized water before further tests.

Nanobubble enhanced polyamide membrane at "high concentration". A freshly prepared 2.0 wt.% MPD aqueous solution was ultrasonicated for 30 min, or added with 6.0 wt.% $NaHCO_3$, or pressurized wtih CO_2 or N_2 at 4.0 bar for 30 min. The pre-treated MPD aqueous solution was then reacted with 0.2 wt.% TMC

following the same interfacial polymerization procedures.

Nanobubble eliminated polyamide membrane at "high concentration": A freshly prepared 2.0 wt.% MPD aqueous solution was degassed for 30 min under vacuum. The pre-treated MPD aqueous solution was then reacted with 0.2 wt.% TMC following the same interfacial polymerization procedures.

Polyamide membrane at "low concentration". MPD aqueous solution with a concentration of 0.1 wt.% and TMC hexane solution with a concentration of 0.005 wt.%, a condition referred as "low concentration", were used to fabricate polyamide membrane following the same interfacial polymerization procedures.

Nanobubble enhanced polyamide membrane at "low concentration". A freshly prepared 0.1 wt.% MPD aqueous solution was ultrasonicated for 30 min, or added with 6.0 wt.% $NaHCO_3$, or treated by a combined $NaHCO_3$ addition and ultrasonication treatment. The pre-treated MPD aqueous solution was then reacted with 0.005 wt.% TMC following the same interfacial polymerization procedures.

Polyamide membrane at sub-zero temperature. A freshly prepared 2.0 wt.% MPD aqueous solution was poured on the top surface of polysulfone substrate. The MPD-soaked substrate was stored at -16 °C for 30 min. Then, a 0.2 wt.% TMC hexane solution was gently poured onto the frozen substrate. An interfacial polymerization duration of 2 min was allowed, before the hexane solution was drained. The dried polyamide membrane was used for further microscopic characterization.

Other polyamide thin film composite membranes. A freshly prepared aqueous solution with piperazine, 1,6-hexanediamine, resorcinol, or 1,6-hexandiol concentration of 2.0 wt.% was reacted with 0.2 wt.% TMC following the same interfacial polymerization procedures.

RESULTS AND DISCUSSION

Nanobubbles tune surface structure. "Ridge-and-valley" structures (**Figure 2,A1-2**) appeared for the polyamide membrane prepared using 2.0 wt.% MPD and 0.2 wt.% TMC, a condition referred as "high concentration" that is typical for the synthesis of commercial reverse osmosis membranes. The average roughness (R_a) was 60.3 nm, as typically observed with polyamide reverse osmosis membranes[15, 23]. TEM images show that these roughness structures were composed of multiple ring-like features (**Figure S1,A3** in **Supporting Information**) corresponding to the nano-sized voids encapsulated in the polyamide layer (**Figure S1**,**A4**). To test our hypothesis that these nanovoids were generated by the release of dissolved gases, we degassed the MPD aqueous solution under vacuum before performing interfacial polymerization. The resulting polyamide membrane had a much smoother surface (R_a=29.1 nm, **Figure 2**,**B1-2**). TEM images show an obvious reduction of nanovoids (**Figure S1**,**B3-4**). Our results suggest that formation of nanovoids can be suppressed by removing the dissolved gases (e.g., degassing of the MPD aqueous solution).

Conversely, we designed different strategies to promote the generation of nanobubbles by (i) ultrasonicating the MPD aqueous solution, (ii) adding $NaHCO_3$ into the MPD aqueous solution, and (iii) increasing dissolved gases in the MPD aqueous solution using pressurized CO_2 and N_2. Among the three approaches, ultrasonication is a routinely used method to generate nanobubbles[24, 25] that remains stable for a significant period of time (on the order of $10^3 – 10^4$ s) in aqueous solutions[26, 27] or at solid-liquid interfaces[28, 29]. In the second approach, $NaHCO_3$ was introduced as a precursor to produce CO_2 by the heat and HCl generated during the interfacial polymerization reaction. In all cases, the polyamide layers had greater extent of large-sized nanovoids (**Figure S2-S3**).

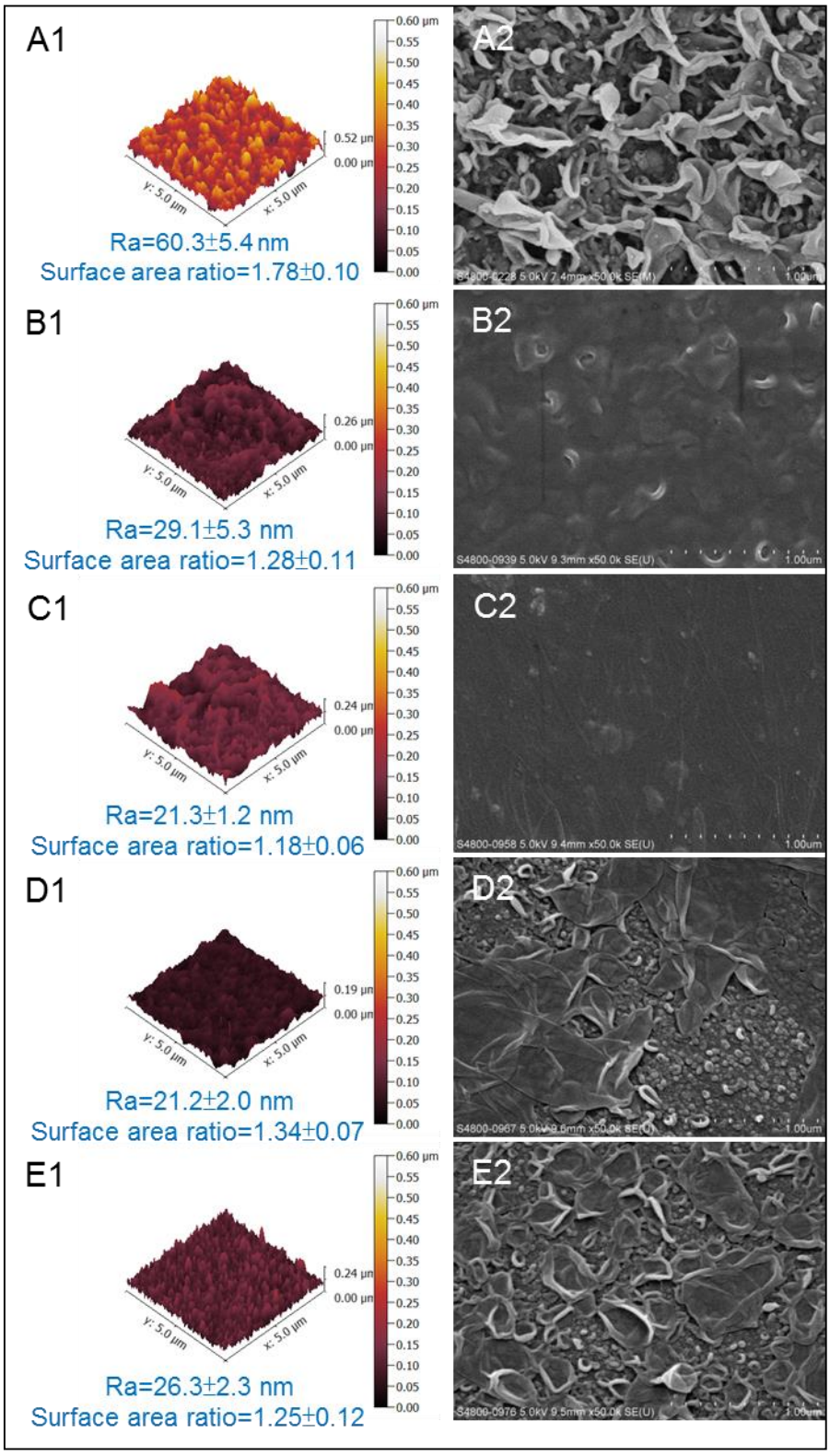

Figure 2. Morphological structures of polyamide thin film with enhanced and eliminated nanobubbles under different MPD and TMC concentrations. (A) 2.0 wt.% MPD aqueous solution interfacially polymerized with 0.2 wt.% TMC hexane solution for 2 min. (B) Degassing of 2.0 wt.% MPD aqueous solution which is then interfacially polymerized with 0.2 wt.% TMC hexane solution for 2 min. (C) 0.1 wt.% MPD aqueous solution interfacially polymerized with 0.005 wt.% TMC hexane solution for 2 min. (D) Ultrasonication of 0.1 wt.% MPD aqueous solution which is then interfacially polymerized with 0.005

wt.% TMC hexane solution for 2 min. (E) Addition of 6.0 wt.% NaHCO3 to 0.1 wt.% MPD aqueous solution which is then interfacially polymerized with 0.005 wt.% TMC hexane solution for 2 min. Left panel presents atomic-force microscopy (AFM) results and right panel presents scanning electron microscope (SEM) images of top surfaces of polyamide thin film composite membranes.

We further performed interfacial polymerization at "low concentration" conditions using 0.1 wt.% MPD and 0.005 wt.% TMC. The resulting polyamide layer had a relatively smooth surface (R_a=21.3 nm) with no obvious presence of nanovoids (**Figure 2**,**C1-2; Figure S1,C3-C4**). This result is consistent with our hypothesis; the reduced heat/HCl generation under low monomer concentration would minimize the formation of nanobubbles. Here we further demonstrate that "ridge-and-valley" structures can be created for the otherwise smooth surface by promoting nanobubble formation. For example, with an ultrasonication treatment of the MPD aqueous solution before interfacial polymerization, both nodular (small nanovoids) and leaf-like (large nanovoids) features appeared on the polyamide surface (**Figure 2**,**D2**). The addition of $NaHCO_3$ to the MPD aqueous solution resulted in even more extensive leaf-like features (**Figure 2,E2**), which can be explained by the enhanced release of CO_2. These leaf-like roughness features appeared to be flattened, probably due to the low mechanical strength of the roughness features formed at low monomer concentrations.

To better understand the role of nanobubbles in membrane surface morphology, we also prepared poly(piperazinamide) membranes by interfacial polymerization of piperazine and TMC (**Figure S4**). Such membranes typically have a much lower surface roughness compared to membranes formed by interfacial polymerization of MPD and TMC[23]. The reduced background roughness of the poly(piperazinamide) membranes allows us to quantify the average size of "roughness nodules", which increased from 13 nm to 23 nm with the addition of $NaHCO_3$.

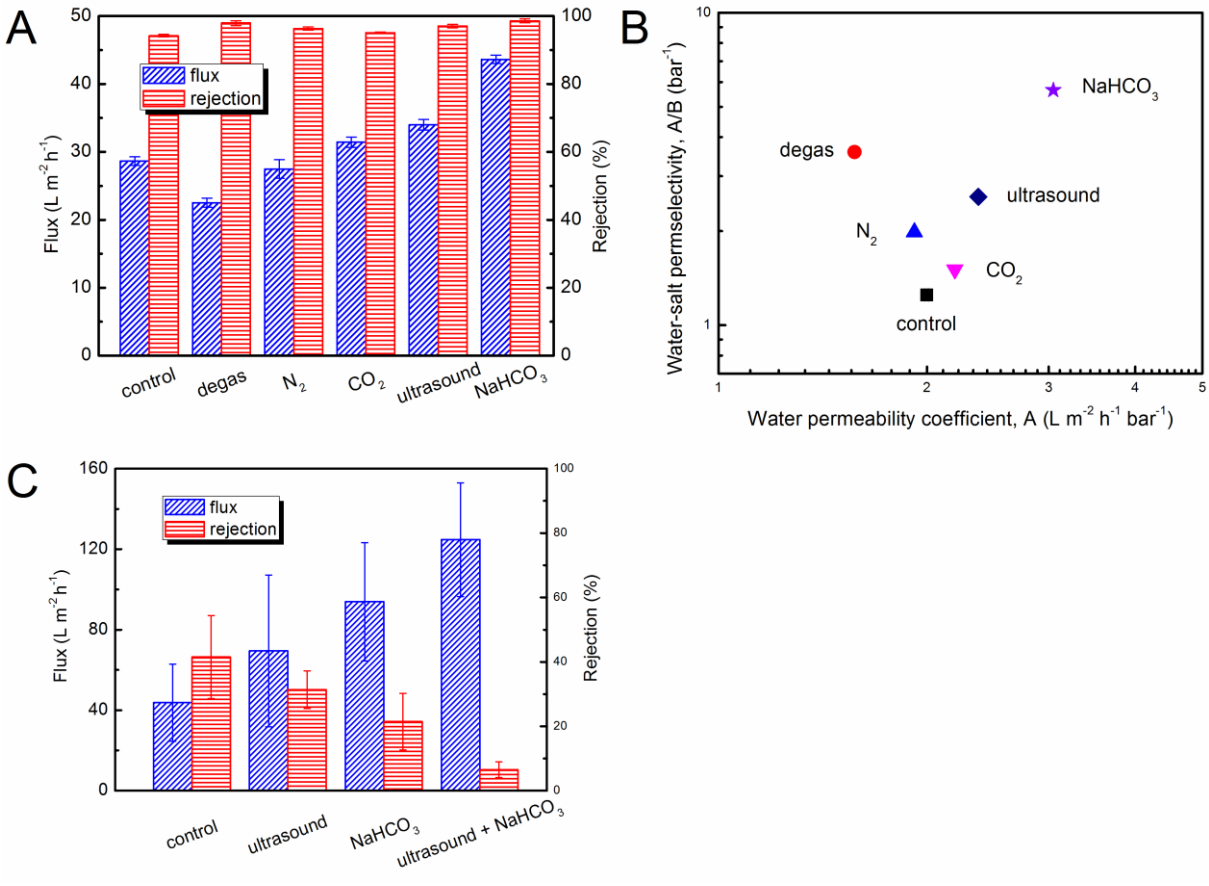

Figure 3. Water and salt transport properties of polyamide thin film composite membranes with enhanced or eliminated nanobubbles. (A) Water flux and salt rejection for "control": 2.0 wt.% MPD aqueous solution interfacially polymerized with 0.2 wt.% TMC hexane solution for 2 min; "degas": degassing of 2.0 wt.% MPD aqueous solution which is then interfacially polymerized with 0.2 wt.% TMC hexane solution for 2 min; "N2" and "CO2": pressuring N2 and CO2 in 2.0 wt.% MPD aqueous solution which is then interfacially polymerized with 0.2 wt.% TMC hexane solution for 2 min, respectively; "ultrasound": ultrasonication of 2.0 wt.% MPD aqueous solution which is then interfacially polymerized with 0.2 wt.% TMC hexane solution for 2 min; "NaHCO3": adding 6.0 wt.% NaHCO3 to 2.0 wt.% MPD aqueous solution which is then interfacially polymerized with 0.2 wt.% TMC hexane solution for 2 min. (B). Plots of water-salt permselectivity, A/B, vs. water permeability coefficient, A for the various membranes tested in part (A). (C) Water flux and salt rejection for "control": 0.1 wt.% MPD aqueous solution interfacially polymerized with 0.005 wt.% TMC hexane solution for 2 min; "ultrasound": ultrasonication of 0.1 wt.% MPD aqueous solution which is then interfacially polymerized with 0.005 wt.% TMC hexane solution for 2 min; "NaHCO3": adding 6.0 wt.% NaHCO3 to 0.1 wt.% MPD aqueous solution which is then interfacially polymerized with 0.005 wt.% TMC hexane solution for 2 min; "NaHCO3 + ultrasound": adding 6.0 wt.% of NaHCO3 in and simultaneously untrasonication of 0.1 wt.% MPD aqueous solution which is then interfacially polymerized with 0.005 wt.% TMC hexane solution for 2 min. All the membranes were evaluated with 2000 mg/L NaCl solution at 16.0 bar and 24 °C with a cross flow velocity of 22.4 cm/s. The effect of concentration polarization has been corrected for the calculation of solute permeability coefficient *B*.

Nanobubbles tune permeability and selectivity. Our results confirm that the nanovoids in the polyamide thin film layer are generated by nanobubbles, a phenomenon we term nano-foaming. Nanobubbles could be removed or generated before or during interfacial polymerization via physical or chemical strategies to endow the polyamide thin film layer with tunable morphologies. The formation or elimination of nanobubbles inside the polyamide thin film also has a marked effect on the membrane's separation properties. For membranes formed at "high monomer concentration" (**Figure 3A**), removal of nanobubbles by degassing the MPD aqueous solution led to a 22% reduction in water flux compared with the control membrane. Conversely, enhanced nanobubble formation resulted in either no change (e.g., using pressurized N_2) or increased water flux (e.g., using pressurized CO_2, ultrasonication, or the addition of $NaHCO_3$). Compared with N_2, CO_2 is much more soluble in water[30], particularly at high pH of the MPD solution (~ 9.3) due to its deprotonation in water to form other soluble species of HCO_3^- and CO_3^{2-}. The lower solubility of N_2 (thus the difficulty to pre-dissolving it in the MPD solution) explains its ineffectiveness in enhancing membrane water flux. Both ultrasonication and $NaHCO_3$ addition led to more obvious flux enhancement of 20% and 52%, respectively. In particular, enhancing nanobubble formation during interfacial polymerization (by $NaHCO_3$ addition) was more effective than pre-generating nanobubbles before interfacial polymerization (by pressurized CO_2 or ultrasonication). Adding $NaHCO_3$, a proton scavenger, may also change the overall IP kinetics and thus the thickness, surface area, and crosslinking of the rejection film. The $NaHCO_3$-addition polyamide had a significantly increased surface roughness (86.3 ±4.9 nm, compared with 60.3 ±5.4 nm for the control membrane) and greater surface area (AFM surface area ratio of 1.92±0.03, compared with 1.78±0.10 for the control), the latter explains the enhancement in water permeability. Assuming a constant volume of polyamide, increasing surface area can reduce the film thickness and thus further improve its water permeability.

We further show that the tailoring of nanobubble formation can enhance water flux without compromising salt rejection. Specifically, we obtained improved salt rejections of 96.6% and 98.6% by ultrasonication and $NaHCO_3$ treatments, respectively, compared with 94.2% of the control membrane. Our results suggest that nanobubble formation does not compromise the integrity of the relatively thick polyamide layer formed at "high monomer concentration". The increased salt rejection with nano-foaming implies a change in the polyamide structure. Additional elemental analysis based on X-ray photoelectron spectroscopy confirms enhanced crosslinking degree of nano-foamed polyamide rejection layers (**Figure S5**)[8, 31]. $NaHCO_3$ served the additional role of H^+ acceptor to promote the interfacial polymerization reaction (**Figure 1A**) in the forward direction with increased crosslinking. **Figure 3B** shows that $NaHCO_3$ addition increased both the membrane water permeability *A* and its selectivity *A/B*, thus breaking the traditional permeability-selectivity tradeoff[10, 32, 33].

Under "low monomer concentration" conditions (**Figure 3C**), a similar trend of increased water flux was observed by promoting nanobubble formation. The water flux was doubled by a combined $NaHCO_3$ addition and ultrasonication treatment. Nevertheless, the concomitant reduction in salt rejection suggests that the membrane integrity was compromised (presence of defects, **Figure S6**) with the formation of nanobubbles in this thinner and less crosslinked polyamide layer[34, 35].

Nano-foaming in a polyamide film depends, to a great extent, on the reactivity and concentration of the monomers. Here we show distinct surface morphologies of rejection films formed by monomers with different activities. MPD exhibited a typical "ridge-and-valley" structure (**Figure 4A**). Piperazine and 1,6-hexanediamine, which are less reactive aliphatic amine monomers, resulted in nodular surface structures (**Figure 4B-C**). Alcohol-based monomers, which form polyesters with TMC, have also been reported in the literature. For example, resorcinol is known to form a rejection layer with a smooth surface[9]. Nevertheless, 1,6-hexandiol

cannot form an intact rejection film (**Figure 4D**) under otherwise similar reaction conditions due to its low reactivity. The formation of large roughness features for the more reactive monomers can be explained by the greater amount of heat released during interfacial polymerization within a shorter period of time (i.e., more rapid reaction). Interestingly, the membrane surface morphology is correlated to the enthalpy of formation $\Delta_f H^{\Theta}_{solid}$ of the monomer (**Figure 4E**).

Lower monomer concentrations can similarly reduce the heat released during the interfacial polymerization and thus reduce the formation of nanobubbles (**Figure 2**,**C2**). An alternative way to reduce the effective concentrations of monomers is to slow down their diffusion rates. We obtained a polyamide film that is nearly free of leaf-like or nodular roughness features by pouring a TMC solution onto a frozen MPD (**Figure S7**) even at "high monomer concentration". In addition, surface roughness can be eliminated by extending the reaction time. In our recent work[36], we prepared, for the first time, a smooth and ultrathin polyamide membrane by electrospraying monomer solutions into fine micro-droplets. The growth rate of the polyamide film (~1 nm/min) was two orders of magnitude slower than conventional ones[37], which allows improved heat dissipation to prevent nanobubble formation[36].

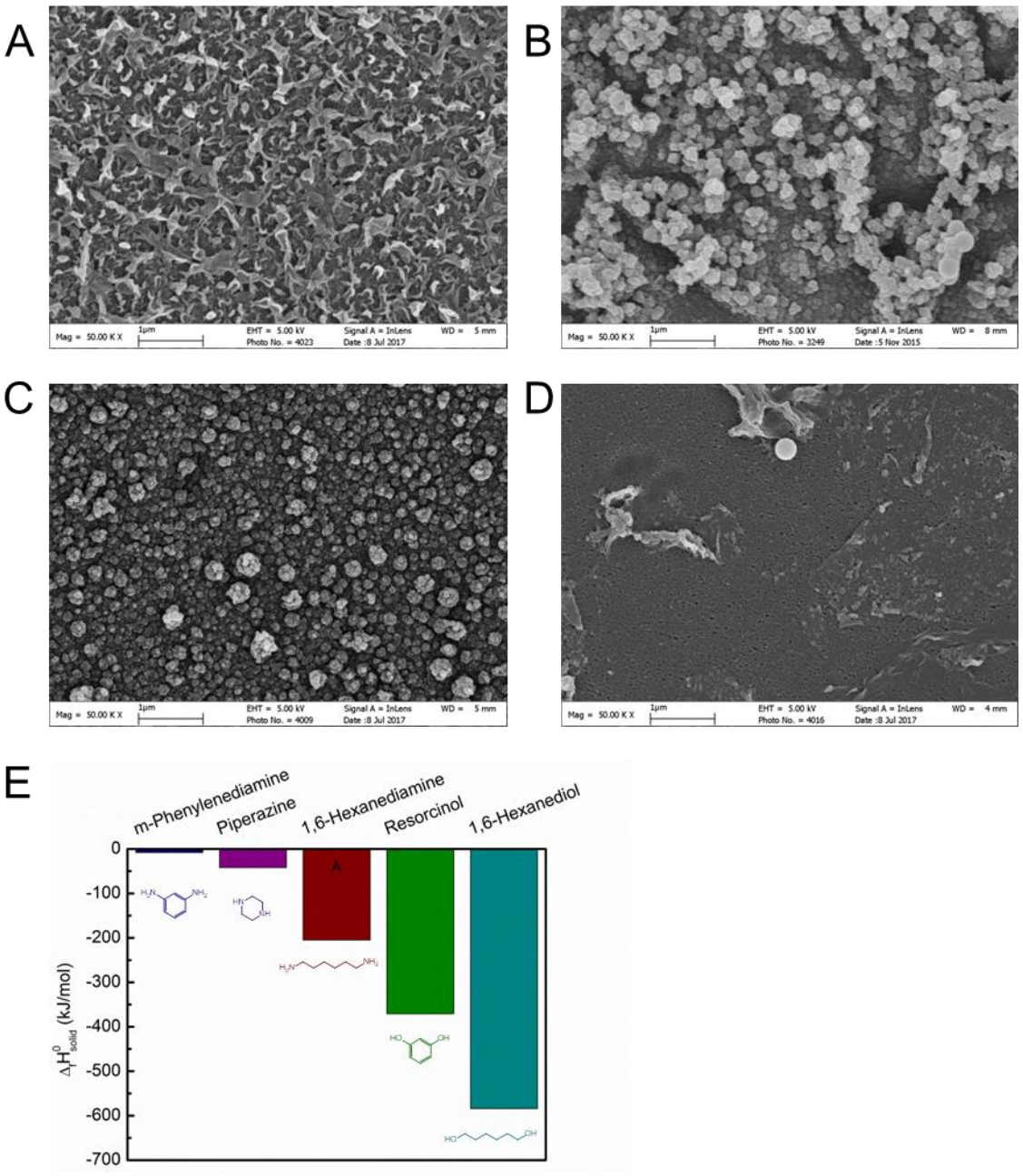

Figure 4. Effect of amine monomer on the morphology of polyamide thin film. Demonstration that amine monomers with greater enthalpy of formation ($\Delta_f H^{\ominus}_{solid}$) release greater amount of heat during interfacial polymerization (with similar monomer concentrations at room temperature), which favors the nano-foaming of polyamide films. SEM images of nanofilms formed by interfacial polymerization of 2.0 wt.% (A) MPD, (B) piperazine, (C) 1,6-hexanediamine, and (D) 1,6-hexanediol with 0.2 wt.% TMC for 2 min. (E) $\Delta_f H^{\ominus}_{solid}$ of amine monomers ($\Delta_f H^{\ominus}_{solid}$ of amine monomer is cited from http://webbook.nist.gov/chemistry/).

In summary, we show that the discrete voids in the thin selective layer of polyamide composite membranes

are generated by dissolved gases. We have demonstrated experimentally via different strategies that nanobubbles could be enhanced or eliminated to tune the structure of polyamide membranes. Specifically, the commonly observed "ridge-and-valley" surface structure formed at "high concentration" can be changed into a smooth one by eliminating the precursor of nanobubbles (e.g., degassing the amine solution) or by reducing the diffusion of the monomers. Conversely, rough membrane surfaces can be formed at "low concentration" by incorporating nanobubbles (e.g., $NaHCO_3$ addition or ultrasonication). The nanobubble-foamed rejection layer simultaneously enhance water permeability and salt rejection by forming a polyamide film of greater surface area together with greater crosslinking, thus providing a route for breaking the permeability-selectivity tradeoff of desalination membranes.

ASSOCIATED CONTENT

Supporting Information

The Supporting Information is available. Materials, polysulfone porous substrates fabrication, filtration test, morphologies, XPS spectra and integrity of nanobubble enhanced polyamide membranes, SEM of polyamide membranes at sub-zero temperature, and interpreting roughness measurement by AFM.

AUTHOR INFORMATION

Corresponding author

* Email: tangc@hku.hk. Phone: +852 28591976.

Notes

The authors declare no competing financial interests.

ACKNOWLEDGMENTS

Supported by Hong Kong Scholars Program (No. XJ2015015), General Research Fund (Project 17207514) of the Research Grants Council of Hong Kong, the Strategic Research Theme (Clean Energy) and Seed Fund for Collaborative Research at the University of Hong Kong, National Natural Science Foundation of China (21406060), Fundamental Research Funds for the Central Universities (WA1514305) and China Postdoctoral Science Foundation (2016M601527).

REFERENCES

1. Elimelech, M.; Phillip, W. A., The Future of Seawater Desalination: Energy, Technology, and the Environment. *Science* **2011,** *333*, 712-717.
2. Logan, B. E.; Elimelech, M., Membrane-based processes for sustainable power generation using water. *Nature* **2012,** *488*, 313-319.
3. Lively, R. P.; Sholl, D. S., From water to organics in membrane separations. *Nature Materials* **2017,** *16*, 276-279.
4. Li, D.; Wang, H., Recent developments in reverse osmosis desalination membranes. *Journal of Materials Chemistry* **2010,** *20*, 4551-4566.
5. Koros, W. J.; Zhang, C., Materials for next-generation molecularly selective synthetic membranes. *Nature Materials* **2017,** *16*, 289-297.
6. Werber, J. R.; Osuji, C. O.; Elimelech, M., Materials for next-generation desalination and water purification membranes. *Nat Rev Mater* **2016,** *1*, 1-15.
7. Kłosowski, M. M.; McGilvery, C. M.; Li, Y.; Abellan, P.; Ramasse, Q.; Cabral, J. T.; Livingston, A. G.; Porter, A. E., Micro-to nano-scale characterisation of polyamide structures of the SW30HR RO membrane using advanced electron microscopy and stain tracers. *Journal of Membrane Science* **2016,** *520*, 465-476.
8. Karan, S.; Jiang, Z.; Livingston, A. G., Sub–10 nm polyamide nanofilms with ultrafast solvent transport for molecular separation. *Science* **2015,** *348*, 1347-1351.
9. Jimenez-Solomon, M. F.; Song, Q.; Jelfs, K. E.; Munoz-Ibanez, M.; Livingston, A. G., Polymer nanofilms with enhanced microporosity by interfacial polymerization. *Nature Materials* **2016,** *15*, 760-767.
10. Park, H. B.; Kamcev, J.; Robeson, L. M.; Elimelech, M.; Freeman, B. D., Maximizing the right stuff: The trade-off between membrane permeability and selectivity. *Science* **2017,** *356*, 1137-1146.
11. Elimelech, M.; Xiaohua, Z.; Childress, A. E.; Seungkwan, H., Role of membrane surface morphology in colloidal fouling of cellulose acetate and composite aromatic polyamide reverse osmosis membranes. *Journal of Membrane Science*

1997, *127*, 101-109.
12. Kong, C.; Kanezashi, M.; Yamomoto, T.; Shintani, T.; Tsuru, T., Controlled synthesis of high performance polyamide membrane with thin dense layer for water desalination. *Journal of Membrane Science* **2010,** *362*, 76-80.
13. Freger, V., Nanoscale Heterogeneity of Polyamide Membranes Formed by Interfacial Polymerization. *Langmuir* **2003,** *19*, 4791-4797.
14. Lau, W. J.; Ismail, A. F.; Misdan, N.; Kassim, M. A., A recent progress in thin film composite membrane: A review. *Desalination* **2012,** *287*, 190-199.
15. Pacheco, F.; Sougrat, R.; Reinhard, M.; Leckie, J. O.; Pinnau, I., 3D visualization of the internal nanostructure of polyamide thin films in RO membranes. *Journal of Membrane Science* **2016,** *501*, 33-44.
16. Pacheco, F. A.; Pinnau, I.; Reinhard, M.; Leckie, J. O., Characterization of isolated polyamide thin films of RO and NF membranes using novel TEM techniques. *Journal of Membrane Science* **2010,** *358*, 51-59.
17. Lin, L.; Lopez, R.; Ramon, G. Z.; Coronell, O., Investigating the void structure of the polyamide active layers of thin-film composite membranes. *Journal of Membrane Science* **2016,** *497*, 365-376.
18. Ramon, G. Z.; Hoek, E. M. V., Transport through composite membranes, part 2: Impacts of roughness on permeability and fouling. *Journal of Membrane Science* **2013,** *425–426*, 141-148.
19. Kolev, V.; Freger, V., Hydration, porosity and water dynamics in the polyamide layer of reverse osmosis membranes: A molecular dynamics study. *Polymer* **2014,** *55*, 1420-1426.
20. Janssen, L.; Te Nijenhuis, K., Encapsulation by interfacial polycondensation. I. The capsule production and a model for wall growth. *Journal of Membrane Science* **1992,** *65*, 59-68.
21. Yuan, F.; Wang, Z.; Yu, X.; Wei, Z.; Li, S.; Wang, J.; Wang, S., Visualization of the Formation of Interfacially Polymerized Film by an Optical Contact Angle Measuring Device. *The Journal of Physical Chemistry C* **2012,** *116*, 11496-11506.
22. Stumm, W.; Morgan, J. J., *Aquatic chemistry: chemical equilibria and rates in natural waters*. John Wiley & Sons: New York, **2012**, 126.
23. Tang, C. Y. Y.; Kwon, Y. N.; Leckie, J. O., Effect of membrane chemistry and coating layer on physiochemical properties of thin film composite polyamide RO and NF membranes II. Membrane physiochemical properties and their dependence on polyamide and coating layers. *Desalination* **2009,** *242*, 168-182.
24. Zimmerman, W. B.; Tesař, V.; Bandulasena, H. C. H., Towards energy efficient nanobubble generation with fluidic oscillation. *Current Opinion in Colloid & Interface Science* **2011,** *16*, 350-356.
25. Leighton, T., *The Acoustic Bubble*. Academic Press: New York, **1994**.
26. Ohgaki, K.; Khanh, N. Q.; Joden, Y.; Tsuji, A.; Nakagawa, T., Physicochemical approach to nanobubble solutions. *Chemical Engineering Science* **2010,** *65*, 1296-1300.
27. Seo, D.; German, S. R.; Mega, T. L.; Ducker, W. A., Phase State of Interfacial Nanobubbles. *The Journal of Physical Chemistry C* **2015,** *119*, 14262-14266.
28. Yang, S.; Dammer, S. M.; Bremond, N.; Zandvliet, H. J. W.; Kooij, E. S.; Lohse, D., Characterization of Nanobubbles on Hydrophobic Surfaces in Water. *Langmuir* **2007,** *23*, 7072-7077.
29. Zhang, X. H.; Quinn, A.; Ducker, W. A., Nanobubbles at the Interface between Water and a Hydrophobic Solid. *Langmuir* **2008,** *24*, 4756-4764.
30. Kolev, N. I., Solubility of O2, N2, H2 and CO2 in water. In *Multiphase Flow Dynamics 4: Turbulence, Gas Adsorption and Release, Diesel Fuel Properties*, Springer Berlin Heidelberg: Berlin, Heidelberg, **2012**, 209-239.
31. Tang, C. Y. Y.; Kwon, Y. N.; Leckie, J. O., Effect of membrane chemistry and coating layer on physiochemical properties of thin film composite polyamide RO and NF membranes I. FTIR and XPS characterization of polyamide and coating layer chemistry. *Desalination* **2009,** *242*, 149-167.
32. Freeman, B. D., Basis of permeability/selectivity tradeoff relations in polymeric gas separation membranes.

Macromolecules **1999,** *32*, 375-380.
33. Werber, J. R.; Deshmukh, A.; Elimelech, M., The Critical Need for Increased Selectivity, Not Increased Water Permeability, for Desalination Membranes. *Environ Sci Tech Let* **2016,** *3*, 112-120.
34. Chai, G.-Y.; Krantz, W. B., Formation and characterization of polyamide membranes via interfacial polymerization. *Journal of Membrane Science* **1994,** *93*, 175-192.
35. Roh, I. J.; Greenberg, A. R.; Khare, V. P., Synthesis and characterization of interfacially polymerized polyamide thin films. *Desalination* **2006,** *191*, 279-290.
36. Ma, X.-H.; Yang, Z.; Yao, Z.-K.; Guo, H.; Xu, Z.-L.; Tang, C. Y., Interfacial Polymerization with Electrosprayed Microdroplets: Toward Controllable and Ultrathin Polyamide Membranes. *Environmental Science & Technology Letters* **2018,** DOI 10.1021/acs.estlett.7b00566.
37. Song, X.; Qi, S.; Tang, C. Y.; Gao, C., Ultra-thin, multi-layered polyamide membranes: Synthesis and characterization. *Journal of Membrane Science* **2017,** *540*, 10-18.

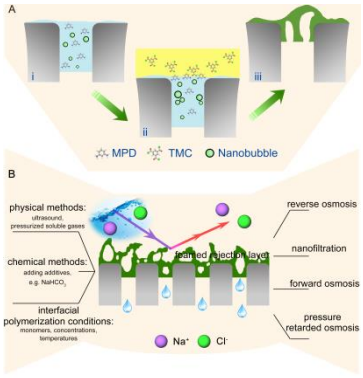
A
i
ii
iii
MPD
TMC
Nanobubble
B
physical methods:
ultrasound,
pressurized soluble gases
chemical methods:
adding additives,
e.g. NaHCO3
interfacial
polymerization conditions:
monomers, concentrations,
temperatures
formed rejection layer
reverse osmosis
nanofiltration
forward osmosis
pressure
retarded osmosis
Na+
Cl-

Supporting Information

Nano-foaming of polyamide desalination membranes to tune permeability and selectivity

Xiao-Hua Ma [†,‡], Zhi-Kan Yao [‡], Zhe Yang [‡], Hao Guo [‡], Zhen-Liang Xu [†], Chuyang Y. Tang*[,‡], Menachem Elimelech [§]

[†] Shanghai Key Laboratory of Multiphase Materials Chemical Engineering, Membrane Science and Engineering R&D Lab, Chemical Engineering Research Center, East China University of Science and Technology, 130 Meilong Road, Shanghai 200237, China

[‡] Department of Civil Engineering, The University of Hong Kong, Pokfulam HW619B, Hong Kong, China

[§] Department of Chemical and Environmental Engineering, Yale University, New Haven, CT 06520-8286

Email: * tangc@hku.hk; phone: +852 2859 1976; fax: +852 2559 5337.

S1. Materials

M-phenylenediamine (MPD, 99%, flakes), sodium bicarbonate ($NaHCO_3$, powder), trimesoyl chloride (TMC, 98%), hexane, polysulfone (average Mw ~ 35,000 by LS, average Mn ~ 16,000 by MO, pellets), N,N-dimethylformamide (for HPLC, ≥ 99.9%), and sodium chloride (NaCl, anhydrous) were purchased from Sigma Aldrich and used without further purification. CO_2 and N_2 were obtained from Hong Kong Special Gases.

S2. Experimental

S2.1 Fabrication of polysulfone porous substrates

Polysulfone solution was prepared by dissolving 15 wt.% (wt./wt.) of polysulfone pellests in N,N-dimethylformamide under stirring at 50 °C. After cooling to room temperature and degassing, the dope solution was casted onto a clean glass plate using an automatic film applicator (Elcometer 4340, UK). The gap between the casting knife and the glass plate was set at 150 μm. The glass plate with thin polysulfone layer was immediately immersed in a deionized water bath, where phase inversion took place. The nascent polysulfone porous substrate was rinsed and soaked with deionized water for at least 24 hours at room temperature before further use. The obtained polysulfone porous substrate had a water permeability of approximately 400 $L \cdot m^{-2} \cdot h^{-1}$.

S2.2 Separation performance of polyamide thin film composite membranes

The flux and rejection performances of polyamide thin film composite membrane were analyzed through a cross-flow filtration system [1, 2]. The membrane was stabilized with 2000 mg/L NaCl feed solution at an operating pressure of 16.0 bar with a crossflow velocity of 22.4 cm/s. During the experiment, the feed solution temperature was controlled at 24 ± 0.1 °C by a circulating chiller. Samples were taken after water flux reached a stable value (approximately 2 hours). The permeation flux was calculated as follows:

$$J_w = \frac{\Delta V}{A_m \cdot \Delta t} \tag{1}$$

where J_w represents permeate flux ($L \cdot m^{-2} \cdot h^{-1}$); ΔV represents total volume of the permeate solution (L), A_m is the effective area of polyamide thin film composite membrane with a value of 14.4 cm^2 in the current work; and Δt is duration of permeation (h).

The salt rejection was calculated by:

$$R = \left(1 - \frac{C_p}{C_f}\right) \times 100\% \tag{2}$$

where C_p and C_f are the concentration of the permeate solution and the feed solution, respectively. In the current work, rejection was calculated by testing the electrical conductivity (Myron L Company, Carlsbad, CA) of the permeate solution and the feed solution.

Water permeability coefficient, A, and solute permeability coefficient, B, were calculated by

$$A = \frac{J_w}{\Delta P - \Delta \pi} \tag{3}$$

$$B = \frac{J_w\left(\frac{1}{R} - 1\right)}{\exp\left(\frac{J_w}{k}\right)} \tag{4}$$

where ΔP represents transmembrane pressure (bar), $\Delta \pi$ is the osmotic pressure of the feed solution (2000 mg/L NaCl). The term $\exp(J_w/k)$ corrects for the concentration polarization effect [3], where the mass transfer coefficient k (8.9×10^{-5} m/s) is calculated in accordance to She et al [4].

S3. TEM results of polyamide membranes with enhanced or eliminated nanobubbles

The surface morphology and cross-sectional structure of the polyamide membranes prepared under different strategies is presented in Figure S1. At “high concentration” conditions, multiple ring-like features (Figure S1, A3) were observed. These features correspond to the nano-sized voids encapsulated in the polyamide layer, resulting in a ridge-and-valley surface morphology (Figure S1, A4). Degassing pre-treatment reduced the formation of nanovoids (Figure S1, B3-4). At “low concentration” conditions, the resulting polyamide layer had a smoother surface (Figure S1, C3-C4). Nano-forming methods, particularly $NaHCO_3$ addition, promoted more ring-like features in TEM top views (Figure S1, E3).

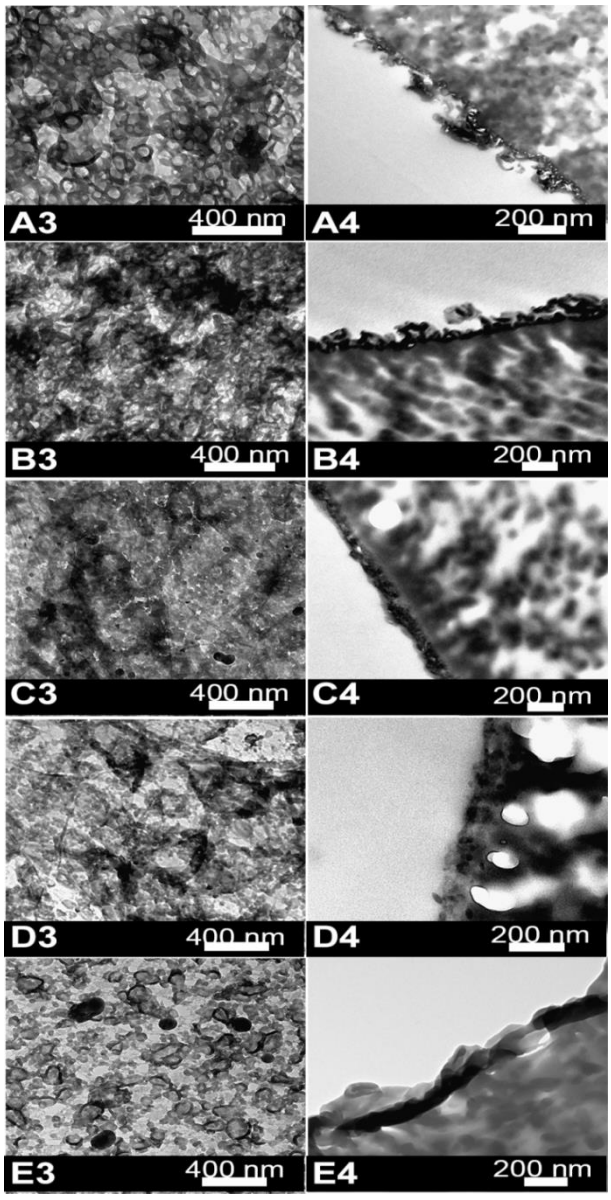

Figure S1. Morphological structures of polyamide thin films with enhanced or eliminated nanobubbles under different MPD and TMC concentrations. (A) 2.0 wt.% MPD aqueous solution interfacially polymerized with 0.2 wt.% TMC hexane solution for 2 min; (B) degasing of 2.0 wt.% MPD aqueous solution which is then interfacially polymerized with 0.2 wt.% TMC hexane solution for 2 min; (C) 0.1 wt.% MPD aqueous solution interfacially polymerized with 0.005 wt.% TMC hexane solution for 2 min; (D) ultrasonication of 0.1 wt.% MPD aqueous solution which is then interfacially polymerized with 0.005 wt.% TMC hexane solution for 2 min; (E) adding 6.0 wt.% $NaHCO_3$ to 0.1 wt.% MPD aqueous solution which is then interfacially polymerized with 0.005 wt.% TMC hexane solution for 2 min; left panel presents TEM images of top surfaces, and right panel presents TEM images of cross-sections of polyamide thin film composite membranes.

S4. Morphologies of nanobubble enhanced polyamide membranes

The morphologies of nanobubble enhanced polyamide membranes are shown in Figure S2 and S3. Larger leaf-like and even belt-like features were observed.

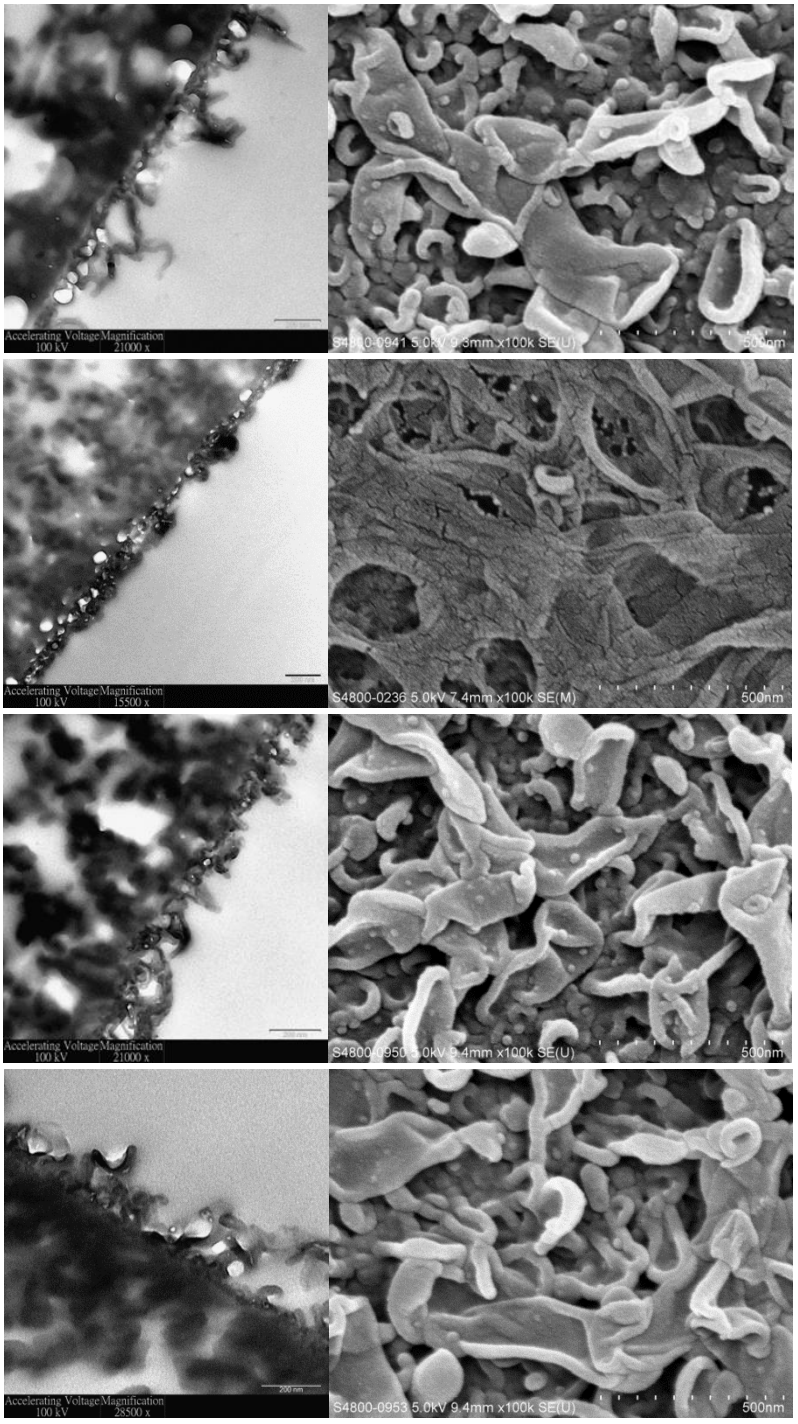

Figure S2. Cross-sectional TEM images and top surface SEM images of polyamide thin film composite membrane enhanced with nanobubbles. (A) ultrasonicating MPD aqueous solution; (B) adding 6.0 wt.% $NaHCO_3$ in MPD aqueous solution; (C) pressuring CO_2 in MPD aqueous solution, and (D) pressuring N_2 in MPD aqueous solution. All polyamide thin film composite membranes were fabricated by interfacial polymerization of 2.0 wt.% MPD aqueous solution and 0.2 wt.% TMC hexane solution for 2 min.

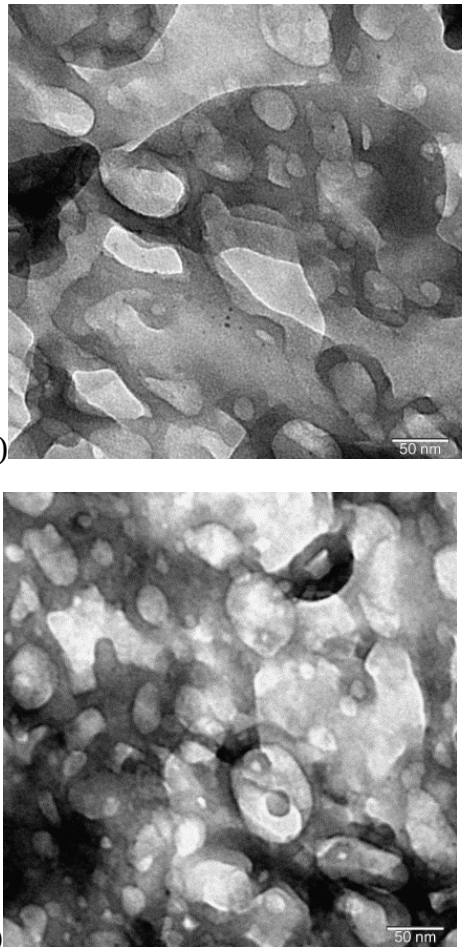

Figure S3. Top surface TEM images of polyamide thin film composite membranes. (A) 2.0 wt.% MPD aqueous solution interfacially polymerized with 0.2 wt.% TMC hexane solution for 2 min; and (B) adding 6.0 wt.% $NaHCO_3$ in 2.0 wt.% MPD aqueous solution which is then interfacially polymerized with 0.2 wt.% TMC hexane solution for 2 min.

To better understand the role of nanobubbles in membrane surface morphology, we also prepared poly(piperazinamide) membranes by interfacial polymerization of piperazine and TMC (Figure S4). The reduced background roughness of the poly(piperazinamide) membranes allows us to quantify the average size of "roughness nodules", which increased from 13 nm to 23 nm with the addition of $NaHCO_3$.

A)

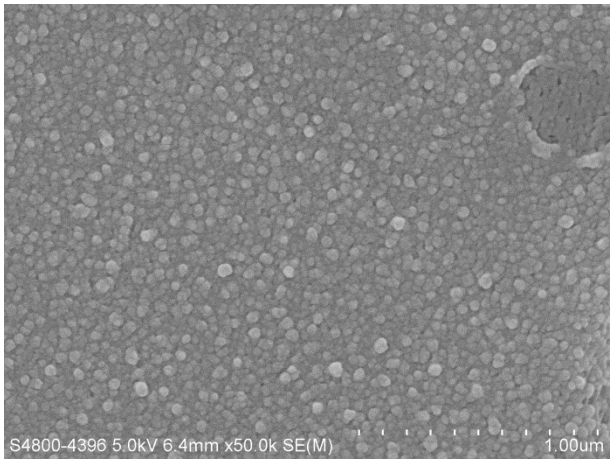

B)

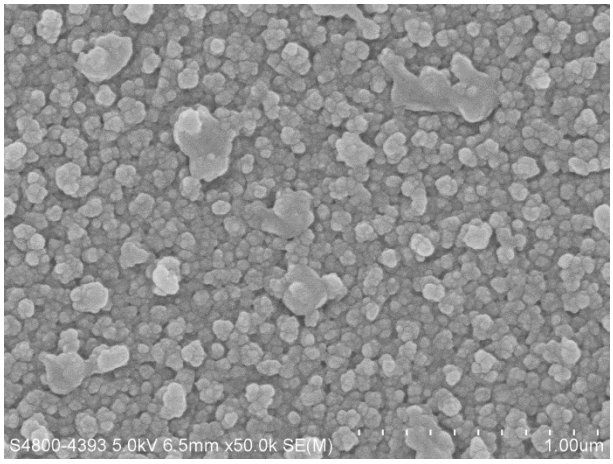

C)

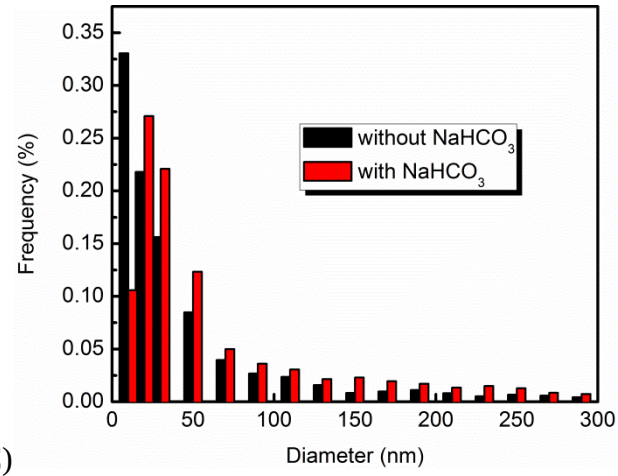

Figure S4. SEM images of poly(piperazinamide) membranes and nodular diameter distribution. (A) 2.0 wt.% piperazine aqueous solution interfacially polymerized with 0.2 wt.% TMC hexane solution for 2 min; (B) adding 6.0 wt.% $NaHCO_3$ in 2.0 wt.% piperazine aqueous solution which is then interfacially polymerized with 0.2 wt.% TMC hexane solution for 2 min; and (C) Nodular diameter distribution diagram, values were obtained by statistics the nodular diameter from SEM images of (A) and (B).

S5. XPS spectra of nanobubble enhanced polyamide membranes

XPS spectra for polyamide thin film composite membranes are presented in Figure S5. The O/N ratio decreased for nanobubble enhanced polyamide membranes, implying an enhanced crosslinking degree. The formation of more cross-linked polyamide explains the increased salt rejection.

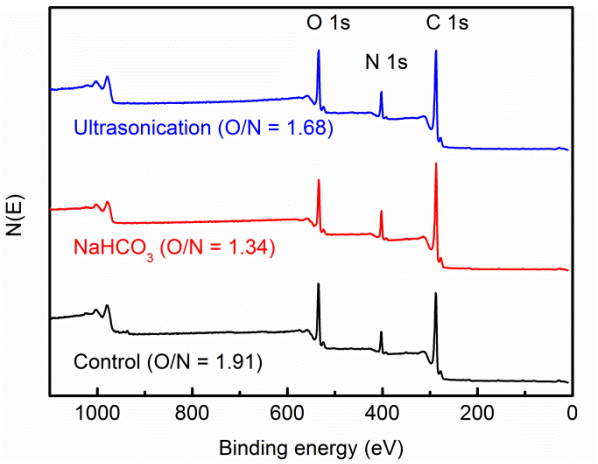

Figure S5. XPS spectra for polyamide thin film composite membranes fabricated by 2.0 wt.% MPD aqueous solution interfacially polymerized with 0.2 wt.% TMC hexane solution for 2 min; ultrasonicating 2.0 wt.% MPD aqueous solution which is then interfacially polymerized with 0.2 wt.% TMC hexane solution for 2 min; and adding 6.0 wt.% $NaHCO_3$ in 2.0 wt.% MPD aqueous solution which is then interfacially polymerized with 0.2 wt.% TMC hexane solution for 2 min.

S6. Integrity of nanobubble enhanced polyamide membranes at "low concentration"

At "low monomer concentration" condition, enhanced formation of nanobubbles with $NaHCO_3$ addition can lead to formation of pinholes in the polyamide rejection layer (Figure S6), which compromises the membrane rejection.

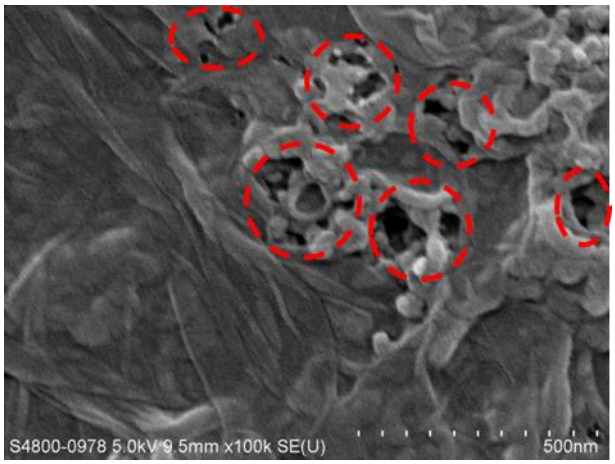

Figure S6. Top surface SEM images of polyamide thin film composite membranes fabricated by adding 6.0 wt.% $NaHCO_3$ in 0.1 wt.% MPD aqueous solution which is then interfacial polymerization with 0.005 wt.% TMC hexane solution for 2 min.

S7. SEM of polyamide membranes at sub-zero temperature

A polyamide film was formed on a frozen MPD-soaked substrate under “high concentration” condition. As shown in Figure S7, the film is nearly free of leaf-like or nodular roughness features.

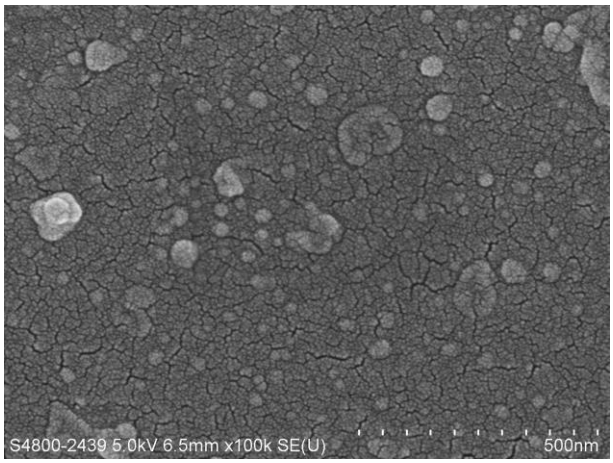

Figure S7. SEM image of polyamide thin film composite membrane fabricated by interfacial polymerization of a frozen 2.0 wt.% MPD aqueous solution (at -16 °C) with a 0.2 wt.% TMC hexane solution for 2 min.

S8. Interpreting roughness measurement by AFM

It is important to understand the principle of AFM roughness measurement. AFM basically measures the sample height Z_i at each point i over an array of points. The average roughness is calculated by $(\Sigma|Z_i - Z_{ave}|)/n$, where Z_{ave} is the average sample height and n is the total number of measuring points. Consider an atomically smooth surface (Figure S8A). Ideally, its roughness value is zero. However, if there is any curvature of the surface (say due to sample mounting), the AFM technique will still measure a roughness value. In this case, the measured AFM roughness is only a reflection of the sample curvature, not the intrinsic surface roughness. For a sample with relatively low intrinsic surface roughness (Figure S8B), its roughness effect will be over-dominated by the curvature effect. For a sample containing relatively rough features (Figure S8C), the intrinsic roughness effect will over-shadow the curvature effect, such that the measured AFM roughness becomes a better reflection of the intrinsic surface roughness. As such, it is important to use both SEM and AFM to interpret the results, particularly for samples with relatively smooth surface.

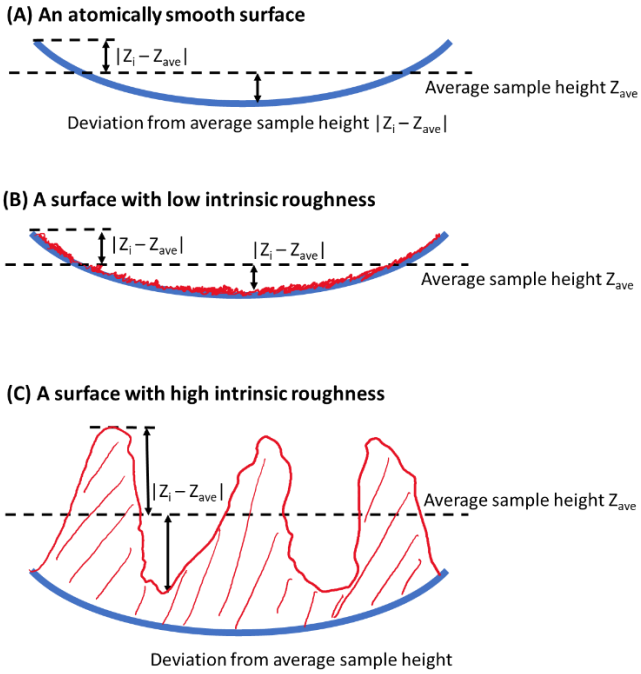

Figure S8. Illustration of AFM roughness measurement for (A) an atomically smooth surface, (B) a surface with low intrinsic roughness, and (C) a surface with high intrinsic roughness.

Reference list

1. Tang, C. Y.; Kwon, Y.-N.; Leckie, J. O., Fouling of reverse osmosis and nanofiltration membranes by humic acid-Effects of solution composition and hydrodynamic conditions. *Journal of Membrane Science* **2007,** *290*, 86-94.
2. Ma, X.-H.; Yang, Z.; Yao, Z.-K.; Xu, Z.-L.; Tang, C. Y., A facile preparation of novel positively charged MOF/chitosan nanofiltration membranes. *Journal of Membrane Science* **2017,** *525*, 269-276.
3. Fane, A. G.; Tang, C. Y.; Wang, R., 4.11 - Membrane Technology for Water: Microfiltration, Ultrafiltration, Nanofiltration, and Reverse Osmosis A2 - Wilderer, Peter. In *Treatise on Water Science*, Elsevier: Oxford, **2011**, 301-335.
4. She, Q. H.; Hou, D. X.; Liu, J. X.; Tan, K. H.; Tang, C. Y. Y., Effect of feed spacer induced membrane deformation on the performance of pressure retarded osmosis (PRO): Implications for PRO process operation. *Journal of Membrane Science* **2013,** *445*, 170-182.